ACS APPLIED MATERIALS & INTERFACES

Research Article

www.acsami.org

Formation Mechanism and Control of Perovskite Films from Solution to Crystalline Phase Studied by in Situ Synchrotron Scattering

Chun-Yu Chang,[†] Yu-Ching Huang,[‡] Cheng-Si Tsao,*[,†,‡] and Wei-Fang Su*[,†]

[†]Department of Materials Science and Engineering, National Taiwan University, Taipei 10617, Taiwan

[‡]Institute of Nuclear Energy Research, Taoyuan 32546, Taiwan

Supporting Information

ABSTRACT: Controlling the crystallization and morphology of perovskite films is crucial for the fabrication of high-efficiency perovskite solar cells. For the first time, we investigate the formation mechanism of the drop-cast perovskite film from its precursor solution, $PbCl_2$ and CH_3NH_3I in *N*,*N*-dimethylformamide, to a crystalline $CH_3NH_3PbI_{3-x}Cl_x$ film at different substrate temperatures from 70 to 180 °C in ambient air and humidity. We employed an in situ grazing-incidence wide-angle X-ray scattering (GIWAXS) technique for this study. When the substrate temperature is at or below 100 °C, the perovskite film is formed in three stages: the initial solution stage, transition-to-solid film stage, and transformation stage from intermediates into a crystalline perovskite film. In each stage, the multiple routes for phase transformations are preceded concurrently. However, when the substrate temperature is increased from 100 to 180 °C, the formation mechanism of the perovskite film is changed from the "multistage formation mechanism" to the "direct formation mechanism". The proposed mechanism has been applied to understand the formation of a perovskite film containing an additive. The result of this study provides a fundamental understanding of the functions of the solvent and additive in the solution and transition states to the crystalline film. It provides useful knowledge to design and fabricate crystalline perovskite films for high-efficiency solar cells.

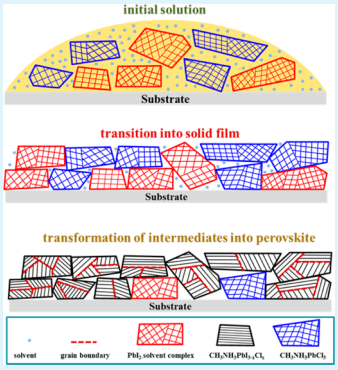

KEYWORDS: *grazing-incidence wide-angle X-ray scattering (GIWAXS), crystallization kinetics, formation mechanism, perovskite, solar cell*

INTRODUCTION

Organic−inorganic hybrid perovskite materials with a chemical composition of ABX_3 (A = organic cation; B = metal cation; X = Cl, Br, or I) have attracted significant attention because of their outstanding optical and electrical properties.[1−4] Photovoltaics based on the ABX_3 perovskite structure have rapidly developed in the past few years, and the power conversion efficiency (PCE) has recently achieved a certified PCE of 22.1%.[5] The literature reports many methods to prepare the perovskite absorption layer by solution deposition,[6−15] chemical vapor deposition,[16−18] vapor-assisted solution process,[19,20] and thermal vapor deposition.[21,22] Among these methods, solution deposition is the most promising process for commercialization because it is a low-cost process using less energy and inexpensive equipment and is suitable for mass production. Two kinds of solution methods have been developed: (1) one-step deposition,[6−10] (2) two-step sequential deposition.[11−15] The PCEs of perovskite solar cells reach 19.3%[23] and 20.1%[24] by one-step deposition and two-step sequential deposition, respectively. The one-step deposition is a simpler method to fabricate the perovskite layer for light absorption. In this method, CH_3NH_3X and PbX_2 in *N*,*N*-dimethylformamide (DMF) solvent are mixed to form a precursor solution that is then deposited onto the substrate. In comparison, a two-step deposition process requires to deposit a PbX_2 film first onto the substrate followed by a second deposition of a CH_3NH_3X. The photovoltaic properties and PCEs of the one-step perovskite solar cells can be tailored or optimized by changing the molar ratio of reactants,[25] concentration of the precursor solutions,[26] substrate temperature, and the well-known post thermal annealing.[27] The most studied perovskites are $CH_3NH_3PbI_3$ and $CH_3NH_3PbI_{3-x}Cl_x$. The $CH_3NH_3PbI_3$ and $CH_3NH_3PbI_{3-x}Cl_x$ films are prepared by mixing PbI_2 and $PbCl_2$ with an excess of CH_3NH_3I, respectively. The two perovskites have almost the same crystal structures because x is usually very small.[28] However, the incorporation of a small amount of chlorine in the film of $CH_3NH_3PbI_{3-x}Cl_x$ increases its length of charge diffusion (i.e., chlorine effect),[25,28] which significantly improves the film quality and morphology, leading to improved photovoltaic properties. The crystalline quality and morphology of the perovskite layer are critical to the photovoltaic performance of solar cells.[25−28] They can be controlled by the processing conditions of one-step deposition. The crystallization mechanism of perovskite plays a key role in determining the morphology, internal structure, and growth evolution of its thin film.

Received: June 20, 2016
Accepted: September 16, 2016
Published: September 16, 2016

DOI: 10.1021/acsami.6b07468
ACS Appl. Mater. Interfaces 2016, 8, 26712−26721

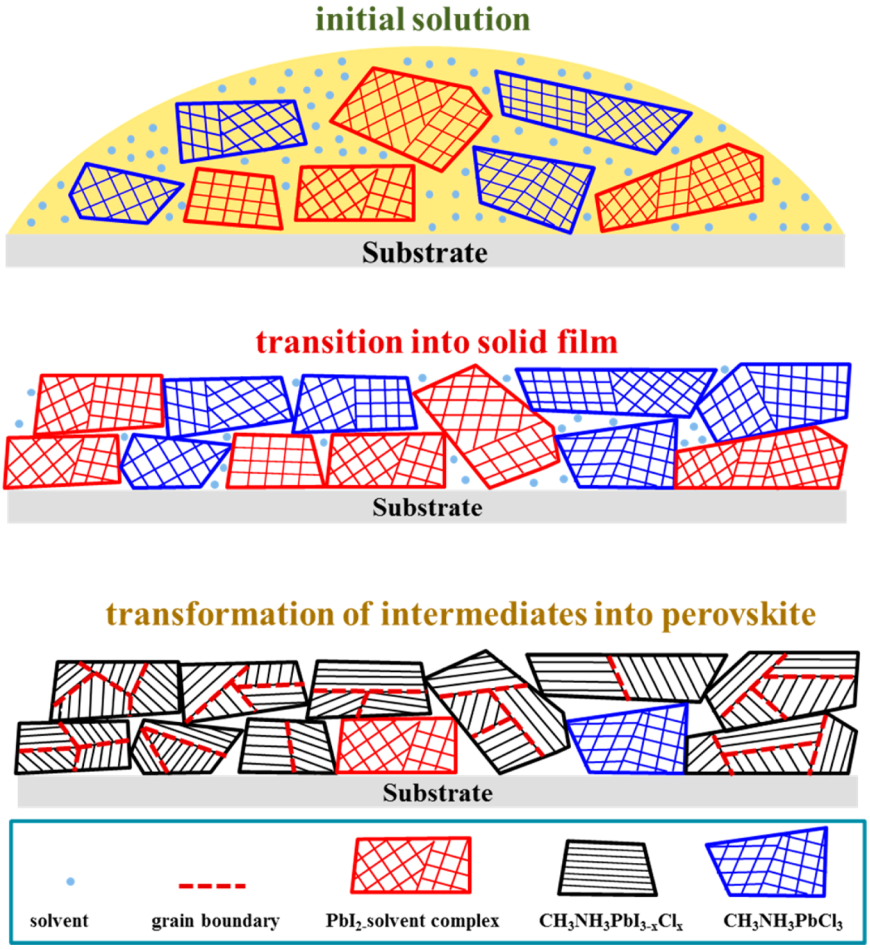

Figure 1. Schematic representation of each stage in a multistage formation mechanism of the perovskite film. Stage I: "initial solution" state. Stage II: "transition into solid film" dry film state. Stage III: "transformation of intermediates into perovskite" film state.

Yang et al.[23] recently demonstrated an enhanced PCE of 19.3% for a perovskite layer formed through a "humidity-assisted reconstruction process" in an atmosphere with a relative humidity of about 30%. In this humidity-assisted process, the formation of a $CH_3NH_3PbCl_3$ intermediate was observed in a thermally annealed film by an X-ray diffraction (XRD) study. However, this intermediate was absent in the conventional dry-air process. In this dry-air process without any humidity or water, the mechanism of $CH_3NH_3PbI_{3-x}Cl_x$ perovskite film formation was predominately through the gradual consumption and transformation of a PbI_2−solvent complex phase during thermal annealing.[26,29] The presence of this PbI_2−solvent complex phase in the precursor solution was confirmed by grazing-incidence wide-angle scattering (GI-WAXS).[26,29] It was speculated that the humidity or water molecules can enhance the reconstruction of a perovskite film during thermal annealing by partially dissolving the reactants and accelerating mass transport within the film.[23] Jen et al.[30] pointed out that the intermediate phase $CH_3NH_3PbCl_3$ played a key role in the formation of the final perovskite structure through phase transformation between the initial precursor and intermediates. However, detailed information and in-depth analysis of the humidity-assisted reconstruction mechanism, including the formation of an intermediate phase of $CH_3NH_3PbCl_3$, are lacking.

The time-dependent GIWAXS technique using two-dimensional (2D) detector is an effective tool in characterizing the evolution of the crystalline structure or phase transformation of a $CH_3NH_3PbI_{3-x}Cl_x$ perovskite film during thermal annealing.[26,29] Grätzel et al.[31] reported that, at an annealing temperature of less than 100 °C for a short time, the transformation of the precursor phase into the perovskite phase in the dry precursor film was incomplete. On the other hand, Mohite et al.[31] developed the "hot-casting" technique by depositing the precursor on the 180 °C substrate to form a perovskite film directly without post-treatment. The high substrate temperature enhanced the formation of $CH_3NH_3PbI_{3-x}Cl_x$ by inducing growth of the perovskite crystalline phase, and thus their device exhibited a good PCE of 18%.[27] However, the mechanism of film formation or phase separation of the perovskite film cast on the hot substrate from the solution state to the final crystalline film is still unknown.

In this paper, we present a comprehensive kinetic study of the mechanism for perovskite film formation at different substrate temperatures employing an in situ synchrotron GIWAXS technique.[32−36] We probe the temporal structural evolution of a one-step, drop- or solution-cast perovskite film, from the precursor solution state to the final crystalline film, at substrate temperatures from 70 to 180 °C in ambient air and humidity (the relative humidity is about 40% at room temperature). The results suggest that the growth mechanism of a perovskite film at 100 °C or below involves three stages: (I) solution stage for the formation of a solution mixture of a PbI_2−solvent complex and $CH_3NH_3PbCl_3$ intermediates, (II)

DOI: 10.1021/acsami.6b07468
ACS Appl. Mater. Interfaces 2016, 8, 26712−26721

transition stage from a solution mixture to a solid mixture of intermediates; (III) phase transformation stage from intermediates to a crystalline perovskite of $CH_3NH_3PbI_{3-x}Cl_x$. At 140 °C and higher, the perovskite film is formed by a "direct formation mechanism". We clearly identify the origin of crystal formation and the types of crystallites in each stage. Furthermore, on the basis of our proposed mechanism, we delineate the crystal formation of a perovskite film from a precursor solution containing a poly(ethylene glycol) (PEG) additive.[37] The knowledge of the mechanism of perovskite film formation provides guidance to optimize the film formation by controlling the temperature and humidity. The mechanistic understanding also yields insight into control of the intermediate phases and perovskite growth toward the design of a cost-effective fabrication process for commercialization of the perovskite solar cell in ambient conditions.

RESULTS AND DISCUSSION

We use the time-dependent in situ synchrotron GIWAXS technique[32−36] to probe the temporal structural evolution from the precursor solution state to the final crystalline perovskite film in a one-step, drop-cast process. In this process, the substrates are heated to temperatures varying from 70 to 180 °C in ambient air and humidity (the relative humidity is about 40% in ambient temperature). The orientations of both the intermediates and perovskite grains throughout the process starting from the precursor solution to the final film formation are revealed by 2D GIWAXS patterns.

Our results provide comprehensive evidence to interpret the formation of intermediates and the film-forming process by a drop-casting process at different temperatures in ambient conditions. Figure 1 illustrates the proposed mechanism for the growth of a perovskite film from solution at 100 °C or lower. The mechanism involves (I) an initial solution stage for the formation of a solution mixture of a PbI_2−solvent complex and $CH_3NH_3PbCl_3$, (II) a transition stage from the solution mixture to a solid mixture of intermediates, and (III) a phase transformation stage from intermediates to a crystalline perovskite of $CH_3NH_3PbI_{3-x}Cl_x$.

At a Substrate Temperature of 70 °C. We use the in situ GIWAXS method to study the structural evolution and phase transformation of the planar $CH_3NH_3PbI_{3-x}Cl_x$ perovskite-film-forming process at 70 °C, which is below the conventional annealing temperature of 100 °C. Figure 2a shows the scattering data of the 70 °C film expressed by the time-dependent profile of the GIWAXS signal integrated from the 2D GIWAXS patterns as a function of the scattering vector Q. The peaks at Q = ∼4, ∼8, and ∼8.7 nm^{-1} are attributed to a PbI_2−solvent complex.[29] The peak at Q = 12.0 nm^{-1} corresponding to XRD with 2θ = 16.9° is assigned to the intermediate phase of $(CH_3NH_3)_{x+y}PbI_{2+x}Cl_y$ or a $CH_3HN_3PbCl_3$−solvent complex.[25] The characteristic behavior of this peak is very similar to that of $CH_3NH_3PbCl_3$ with 2θ = 15.6° reported by Yang et al.[23] For simplicity of expression, we roughly assume that $(CH_3NH_3)_{x+y}PbI_{2+x}Cl_y$ is equivalent to $CH_3NH_3PbCl_3$.[25]

Figure 2b is a plot of the peak intensities of $CH_3NH_3PbI_{3-x}Cl_x$ and intermediate phases versus time during the film formation process. From the data, the process is best rationalized by the three stages illustrated in Figure 1. Evaporation of the DMF solvent takes time at this low temperature. Thus, during t = 0−8 min (stage I, an initial solution stage), the solution stays in the liquid phase and the

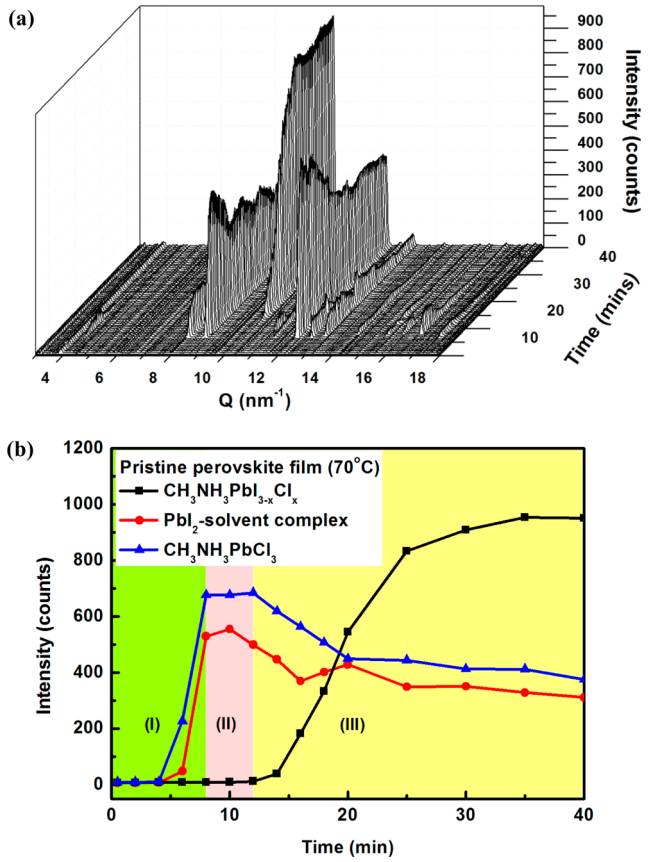

Figure 2. (a) Time-dependent GIWAXS profiles of the pristine perovskite film drop-cast on the 70 °C substrate from solution to solid state (0−40 min). (b) Variation of the index peak intensities of $CH_3NH_3PbI_{3-x}Cl_x$ and intermediate phases with time.

cast film is wet. At t = 4 min, intermediate products (PbI_2−solvent complex and $CH_3NH_3PbCl_3$) are identified. At t = 8 min, they grow into the respective sizes of 64.42 and 54.87 nm, which are calculated from the full width at half-maximum (fwhm) of the peaks (Σ), according to the equation Δ (crystal size) = $2\pi/\Sigma$.[33,34] The sizes of both crystallites are larger than those obtained in the subsequent stages. The formations of the PbI_2−solvent complex and $CH_3NH_3PbCl_3$ crystallites are rapid and are completed in the solution stage rather than in the solid film (shown later). Apparently, solvent assists the rapid nucleation and growth of all crystallites in solution through the effective diffusion and good interaction of precursors. This insight points out that we can control the amount of intermediates effectively by fine-tuning the variables of the initial solution stage, such as temperature, concentration, etc. We also predict that only small amounts of intermediates would be formed in the same amount of time if the film is deposited at room temperature.

When the reaction time was extended from 8 to 12 min, the wet film progressed into stage II, a transition stage from liquid to solid. In this stage, the formations of both crystallites are complete, as evidenced by the lack of change of the corresponding peak intensities in Figure 2b. However, both crystallites are in a metastable state. In Stage II, visual inspection shows the presence of solid-state, semiwet film. Because most of solvent is evaporated from the wet film in this stage, the growth of both $CH_3NH_3PbCl_3$ and PbI_2−solvent complex crystallites is retarded for lack of solvent-assisted

DOI: 10.1021/acsami.6b07468
ACS Appl. Mater. Interfaces 2016, 8, 26712−26721

molecular diffusion. However, the fwhm values of the intermediates continue to increase, indicating a change of ordered structures inside the metastable crystallites, as depicted in Figure 1. To explain this observation, we postulate that the evolution of perovskite is the result of a rearrangement or transformation of the intermediate structure with the help of residual solvent molecules. Furthermore, this stage must be closely affected by the rate of solvent evaporation to form the dry film.

After 12 min of reaction time, the film is in stage III, a phase transformation stage, where the perovskite phase begins to form through transformation of the intermediates. In Figure 2a, the peak at Q = 10.2 nm^{-1}, corresponding to XRD with 2θ = 14.3°, is attributed to the perovskite phase.[26,29] As shown in stage III of Figure 2b, the peak intensity of the perovskite phase increases as both peak intensities of the intermediate crystallites (PbI_2–solvent complex and $CH_3NH_3PbCl_3$) decrease. These behaviors show that crystallization of the perovskite phase proceeds mainly in this stage. It implies that the length of time needed to remove most of the solvent, i.e., the evaporation rate, is a critical controlling factor for the formation of embryonic crystallites at low temperature. Thus, we may optimize the performance of the perovskite layer by controlling the evaporation rate in a low-temperature, drop-cast method.

In stage III, two routes for the phase transformation from intermediates to perovskite crystallites proceed independently and simultaneously in the solid-state film.[23,26] The first route is the formation of perovskite crystallites from the $CH_3NH_3PbCl_3$ intermediate. Decomposition of the $CH_3NH_3PbCl_3$ crystal may release gaseous CH_3NH_3Cl[25] and $PbCl_2$, which interacts with the residual CH_3NH_3I to form $CH_3NH_3PbI_{3-x}Cl_x$. This route is in agreement with the humidity-assisted crystallization mechanism proposed by Yang et al.[23] The second route is the transformation of the PbI_2–solvent complex into the perovskite phase by reaction with $CH_3NH_3^+$ cations. In this process, the excess cations are intercalated into a PbI_2 network, showing the gradual consumption of the PbI_2–solvent complex with decreasing peak intensity and the growth of perovskite with increasing peak intensity (Figure 2b). The second route is in agreement with the common formation mechanism of perovskite crystallites under a nitrogen environment.[26]

The sizes of the PbI_2–solvent complex, $CH_3NH_3PbCl_3$, and perovskite crystallites at the reaction time of 40 min are 61.78, 51.92, and 49.67 nm, respectively, calculated by their fwhm values. The crystal sizes of the two intermediates are smaller than those in the initial stage (64.42 and 54.87 nm for the PbI_2–solvent complex and $CH_3NH_3PbCl_3$, respectively). We speculate that, during transformation of the intermediates to the ordered perovskite structure, reorganization of the lattice structure may independently proceed in certain locally favorable zones within the original parent grain. This leads to the splitting of some large parent grains into small grains for subsequent formation of the perovskite phase inside the crystallites and to an increase in the total surface area.

Figure 3 shows the orientations of the perovskite and intermediate crystallites in stages II and III for the precursor–intermediate–perovskite transformation by the 2D GIWAXS patterns. The diffraction spots of the perovskite and intermediate structures are predominantly oriented in the out-of-plane direction, i.e., normal to the film or substrate surface. For example, the (110) plane of the perovskite crystallites, measured by the diffraction spot at Q = 10.2 nm^{-1}, is normal to the out-of-plane direction expressed as Q_z. It is important to note that Figure 3 shows that the main orientations of both the intermediates and perovskite are not changed during the course of the stage II and III transformations.

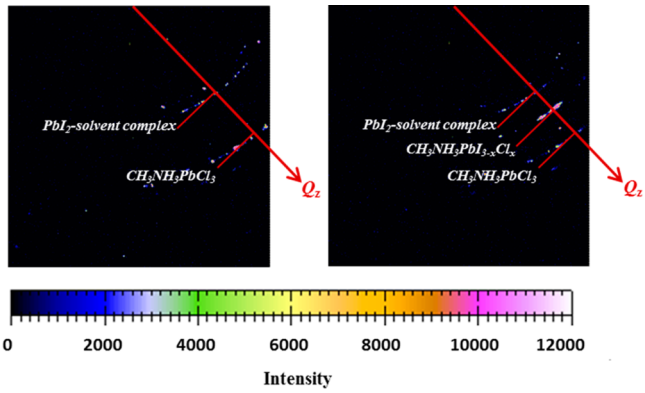

Figure 3. 2D GIWAXS patterns collected at 12 min (stage II, left panel) and 40 min (stage III, right panel). The out-of-plane Q_z direction is marked by a red arrow.

At a Substrate Temperature of 100 °C. In order to understand how the formation mechanism of the perovskite film would change at temperatures higher than 70 °C, we performed a similar in situ GIWAXS study to probe the structural evolution and phase transformation of the drop-cast perovskite film formation at 100 °C. The knowledge obtained from the 70 °C study can be used to predict the intermediates and crystallization kinetics that occurred at these higher temperatures.

Parts a and b of Figure 4 show that the temporal evolution of GIWAXS profiles and index peak intensities of the $CH_3NH_3PbI_{3-x}Cl_x$ film at 100 °C have key features similar to those at 70 °C. Because evaporation of the DMF solvent is faster at 100 °C than at 70 °C, the "initial solution" stage (stage I) occurs during t = 0–2 min. Both intermediates ($CH_3NH_3PbCl_3$ and the PbI_2–solvent complex) are formed quickly at 100 °C in this stage because of the faster reactions at higher temperature. A small amount of perovskite crystallites is also formed in stage I through the transformations of $CH_3NH_3PbCl_3$ and PbI_2–solvent complex intermediates, as indicated by the slight growth of the (110) peak at Q = 10.2 nm^{-1}. Stage II, transition into a solid film, is shortened to t = 4 min. After 4 min, the film formation is in stage III of the transformation. The sizes of the PbI_2–solvent complex, $CH_3NH_3PbCl_3$, and perovskite crystallites at a reaction time of 40 min are 49.94, 46.76, and 34.99 nm, respectively, which are smaller than the sizes in stage I of the initial stage (50.09, 49.27, and 68.48 nm, respectively). This phenomenon can be explained by the same hypothesis as that proposed for the 70 °C process: that the large parent grains split into small grains for subsequent formation of the perovskite phase inside the intermediates.

We also performed the in situ GIWAXS experiment for the pure iodide-based $CH_3NH_3PbI_3$ (PbI_2 + MAI) film at 100 °C with the same deposition conditions for comparison. The temporal evolution of GIWAXS profiles and (110), (220), and (330) peak intensities is shown in Figure S1a,b. The formation and growth behaviors of the $CH_3NH_3PbI_3$ crystal start from 1.6 min in the solution, which is faster than that of the $CH_3NH_3PbI_xCl_{3-x}$ system. The peak of the PbI_2 complex is too weak to detect because of the fast formation of

DOI: 10.1021/acsami.6b07468
ACS Appl. Mater. Interfaces 2016, 8, 26712–26721

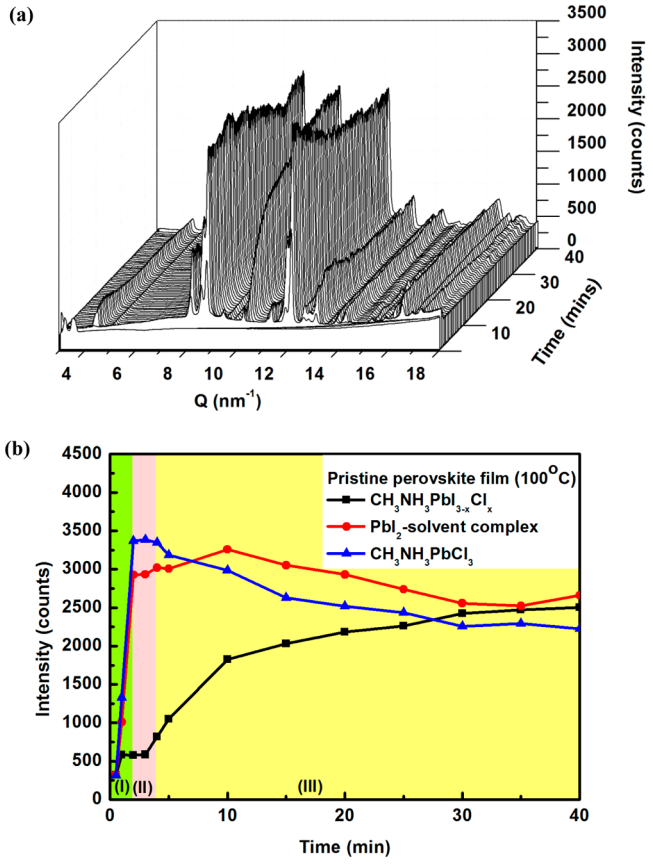

Figure 4. (a) Time-dependent GIWAXS profiles of the pristine perovskite film drop-cast on the 100 °C substrate from solution to solid state (0–40 min). (b) Variation of the index peak intensities of $CH_3NH_3PbI_{3-x}Cl_x$ and intermediate phases with time.

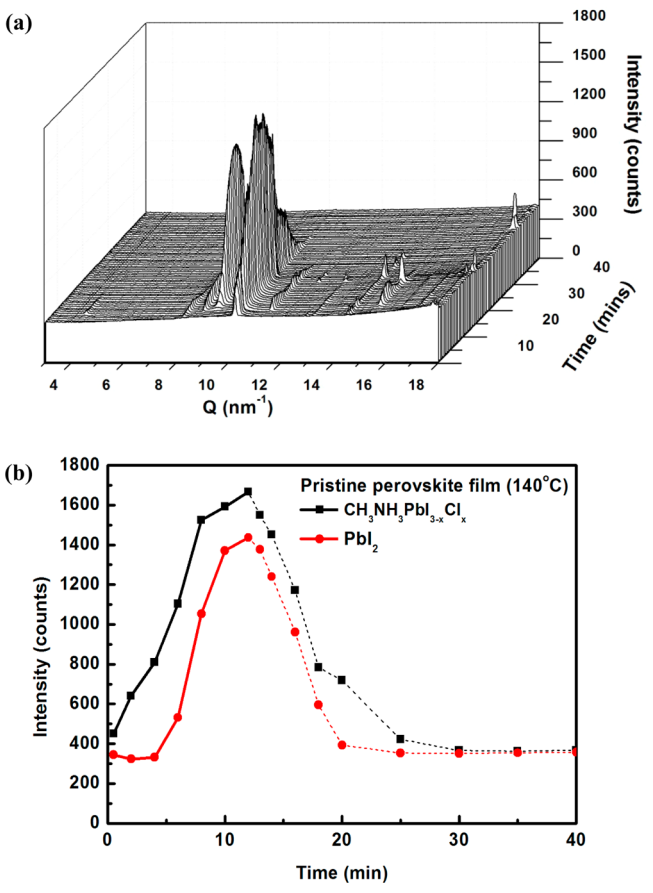

Figure 5. (a) Time-dependent GIWAXS profiles of the pristine perovskite film drop-cast on the 140 °C substrate from solution to solid state (0–40 min). (b) Variation of the index peak intensities of the $CH_3NH_3PbI_{3-x}Cl_x$ and PbI_2 phases with time. Dashed lines show degradation to the amorphous phase.

$CH_3NH_3PbI_3$ directly from PbI_2 with CH_3NH_3I without the interference of $PbCl_2$.

At a Substrate Temperature of over 100 °C (140 and 180 °C, Respectively). Recently, a paper reports a hot-casting technique at 180 °C to produce a large and highly crystalline perovskite film for a high-performance solar cell.[27] However, the crystal formation mechanism at this condition is unknown. This motivates us to study the high-temperature film formation mechanism using the in situ GIWAXS method.

Parts a and b of Figure 5 show the temporal evolution of the GIWAXS profiles and index peak intensities of the $CH_3NH_3PbI_{3-x}Cl_x$ film drop-deposited on a substrate at 140 °C. The profiles and peak intensities in Figure 5 are distinctively different from those in Figure 2 or 4, indicating that the high-temperature crystallization behaviors are different from the multistage transformations at 70 or 100 °C. Parts a and b of Figure 5 show that only the perovskite and PbI_2 phases (at $Q = 9.0$ nm^{-1}) are present at the very early stage at 140 °C. The intermediates observed at 70 or 100 °C, $CH_3NH_3PbCl_3$ and the PbI_2–solvent complex, are absent in the film deposited at 140 °C. The result clearly indicates that, at 140 °C, the two precursor reactants (CH_3NH_3I and $PbCl_2$) directly combine to form a perovskite without any intermediate stage. Earlier, in Figures 2 and 4, we showed that very few perovskite crystallites are formed in stages I and II at substrate temperatures of 100 °C or below. However, at a substrate temperature of 140 °C, the perovskite is formed directly from precursors, by a "direct formation mechanism", which has never been reported in the literature. Remarkably, by providing enough thermal energy and molecular mobility in the hot-casting process, a highly crystalline perovskite film can form directly from solution. At 140 °C, the humidity effect can be ignored because the temperature is high enough to provide sufficient diffusion and interaction of the reactants for perovskite formation. In summary, we observed a remarkable change for perovskite film formation from a "multistage formation mechanism" at low temperature to a "direct formation mechanism" at high temperature.

In Figure 5b, at $t = 5$ min, a peak at $Q = 9.0$ nm^{-1} appears, and its intensity grows with time. This peak is assigned to PbI_2, signifying decomposition of the perovskite phase to PbI_2 due to overheating.[29] The GIWAXS profile shows that the peak of PbI_2 is distinguishable from the peak of the PbI_2–solvent complex (Figure S2). The results indicate that direct formation of the perovskite phase is accompanied by its concurrent decomposition into PbI_2. However, the formation of PbI_2 does not hinder the growth of the perovskite phase. Visual inspection also shows decomposition during formation of the solid film. The solid film with poor thermal conductivity may be favorable for decomposition of the perovskite at the relatively high temperature of 140 °C. When the film on the substrate is heated at 140 °C for more than 12 min (Figure 5b), both the perovskite and PbI_2 phases are degraded rapidly into amorphous structures.

DOI: 10.1021/acsami.6b07468
ACS Appl. Mater. Interfaces 2016, 8, 26712–26721

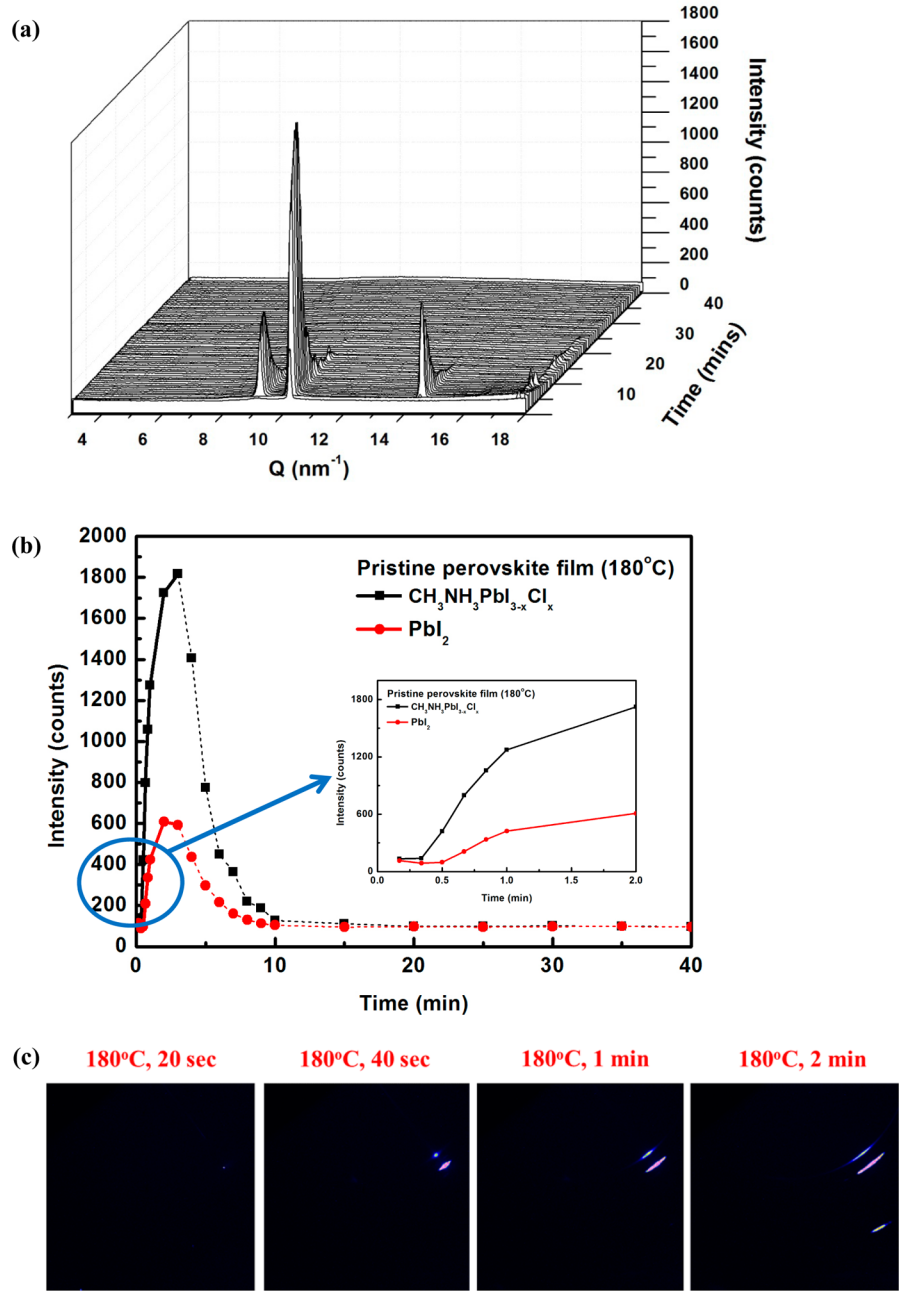

Figure 6. (a) Time-dependent GIWAXS profiles of the pristine perovskite film drop-cast on the 180 °C substrate from solution to solid state (0−40 min). (b) Variation of the index peak intensities of the $CH_3NH_3PbI_{3-x}Cl_x$ and PbI_2 phases with time. (c) 2D GIWAXS patterns selected as representatives.

The temporal evolution of the GIWAXS profiles and index peak intensities of the $CH_3NH_3PbI_{3-x}Cl_x$ film drop-cast on the substrate of 180 °C from solution are shown in Figure 6a,b. We observed a "direct formation mechanism" similar to that at 140 °C but with much faster kinetics. Concurrent decomposition of the perovskite phase into PbI_2 is accelerated and starts at t = 0.5 min because of a 40 °C temperature increase, as indicated by the fast increase of the peak intensity in the expanded graph of Figure 6b. By visual inspection, decomposition into the PbI_2 phase (or formation of the PbI_2 phase) may also occur at the solid-film state. Both the perovskite and PbI_2 phases are seriously degraded after 2.5 min at 180 °C (Figure 6b). It is interestingly noted that, by a comparison of the PbI_2 peak intensities in Figures 5b and 6b, the amount of PbI_2 production is significantly reduced at 180 °C from that at 140 °C. Apparently, the crystallites formed at 180 °C are more dense and stable than those formed at 140 °C because high temperature can accelerate the growth of the perovskite crystallites. Figure 6c shows that the perovskite obtained directly from the solution at 180 °C exhibits high quality with the out-of-plane preferred orientation (narrow angular distribution).

The new finding of "direct formation mechanism" resulted from the fast reaction kinetics. The large perovskite grain obtained from the hot-casting technique[27] may be closely related to the direct formation mechanism without multistage formation via intermediates. How to control the competition between the growth and concurrent decomposition of the

DOI: 10.1021/acsami.6b07468
ACS Appl. Mater. Interfaces 2016, 8, 26712−26721

perovskite phase formed in the direct formation mechanism at high temperature would be critical to tailoring the morphology, crystalline quality, and defect density of the perovskite film.

We further quantitatively analyze the integrated intensity of the $CH_3NH_3PbI_{3-x}Cl_x$ peak at $Q = 10.2$ nm^{-1} as a function of the isothermal heating time. The humidity-assisted crystallization kinetics of the perovskite phase at 70 and 100 °C follow the Avrami law.[26] The model-fitting curves are shown in Figure 7a,b. The fitting equations are $y = 1 - \exp[-0.21(t - 16)^{1.05}]$ at

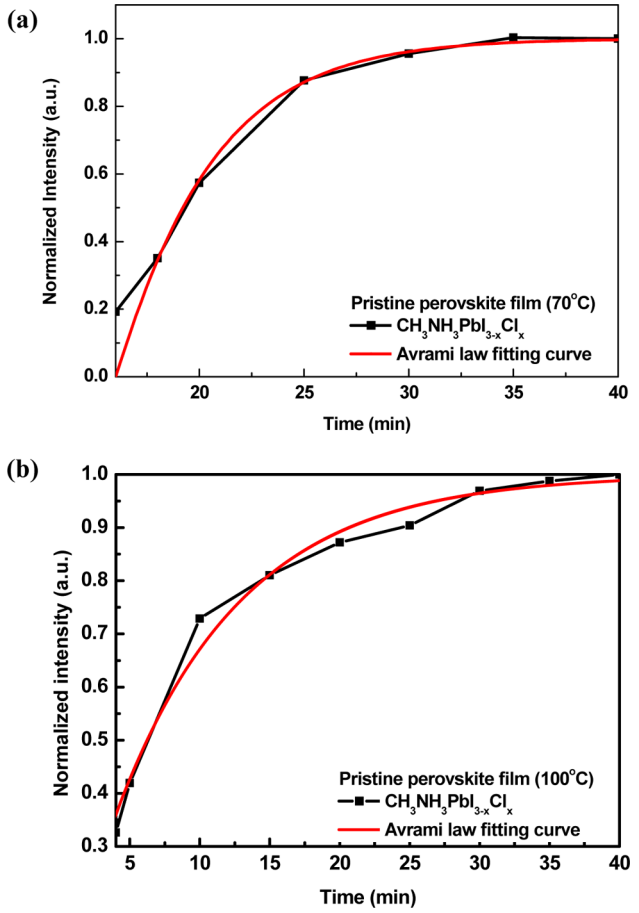

Figure 7. Model-fitting curve of $CH_3NH_3PbI_{3-x}Cl_x$ at substrate temperatures of (a) 70 and (b)100 °C.

$t > 16$ min and $y = 1 - \exp[-0.11(t - 4)^{1.05}]$ at $t > 4$ min when the substrate temperatures are 70 and 100 °C, respectively, where y is the normalized intensity, which is a measure of the transformation fraction, and t is the isothermal heating time. The value of 1.05 is the growth exponent, which is related to the dimensionality of growth and should be between 1 and 4. It is worth mentioning that, because the direct formation of $CH_3NH_3PbI_{3-x}Cl_x$ is too fast at 140 and 180 °C, the data points are not enough for the fitting.

Table 1 summarizes the time-dependent GIWAXS results of a drop-cast perovskite film at different substrate temperatures. On the basis of our proposed mechanisms, we suggest that the best processing condition is at 140 °C for 5 min for a complete phase transformation from solution to perovskite. At the higher temperature of 180 °C, the time can be shortened to 0.5 min, but this time may be too short for good process control during large-scale fabrication.

Effect of the Polymer Additive on the Formation Mechanism of a Perovskite Film from Solution. Figure 8 shows the temporal evolution of the GIWAXS profiles and index peak intensities of the perovskite film prepared from a solution containing 1 wt % PEG and drop-cast at a substrate temperature of 100 °C. The GIWAXS data exhibit characteristics similar to those from a solution without any additive under the same condition. Figure 9 shows the three stages of phase transformation from the solution state to the crystalline film. The time intervals for each stage are the same as those of the processing of the pristine film at the same temperature. However, a discrepancy between the pristine perovskite film and the PEG-containing perovskite film is observed in stage III, "transformation of intermediates into a crystalline perovskite film". In this stage, the perovskite phase in the PEG-containing film reaches a maximum after 25 min, compared with the pristine film after 30 min (Figure 4a,b, indicated by no change of the peak intensity of $CH_3NH_3PbI_{3-x}Cl_x$). The PEG additive is homogeneously distributed in the film and serves as a hindrance site to restrain the growth of intermediate phases. Thus, the sizes of the intermediate crystallites in the PEG-containing film are smaller than those in the pristine film, so the transformation of intermediate to perovskite is faster for the PEG-containing film, as indicated by the shorter time required to reach the peak intensity of $CH_3NH_3PbI_{3-x}Cl_x$.

The grain sizes of both the perovskite and intermediate $CH_3NH_3PbCl_3$ crystallites in the PEG-containing film reach a stable size of ~45 nm at $t > 25$ min. The decrease of the grain size of perovskite crystallites of the pristine film after 4 min at 100 °C is not observed for the PEG-containing film (stage III). This observation implies that the additive can control the grain size of perovskite in the solid film by inhibiting the splitting of the intermediate grain as mentioned above. The planar perovskite solar cell based on the PEG-containing perovskite film therefore shows a better performance of 13.20%, compared to 10.58% based on the pristine perovskite film.[37]

CONCLUSIONS

The in situ GIWAXS technique was employed for the first time to quantitatively elucidate the formation mechanism of the perovskite film from the solution state to the crystalline film by a drop-cast method at substrate temperatures of 70−180 °C in ambient conditions. On the basis of the time-dependent GIWAXS profiles, film formation at 100 °C or below can be characterized by three distinct stages: stage I, an "initial solution stage" with the formation of intermediates in solution, stage II, a "transition into solid film stage" with the evaporation of solvent, and stage III, a "transformation of intermediates into perovskite in the crystalline film stage". At each stage, multiple phase transformations proceed concurrently and can be resolved and characterized by the in situ GIWAXS measurement.

At substrate temperatures below 100 °C, the formation of perovskite crystallites consists of two independent routes. In one route, the $CH_3NH_3PbCl_3$ intermediate decomposes to give CH_3NH_3Cl and $PbCl_2$, which interacts with the residual CH_3NH_3I to form $CH_3NH_3PbI_{3-x}Cl_x$. In the second route, the PbI_2−solvent complex intermediate reacts with $CH_3NH_3^+$ cations to form $CH_3NH_3PbI_{3-x}Cl_x$.

When the substrate temperature is increased to 140 °C or higher, the crystalline perovskite film is formed by a new "direct formation mechanism" with fast kinetics, which is completely different from the "multistage formation mechanism" at

DOI: 10.1021/acsami.6b07468
ACS Appl. Mater. Interfaces 2016, 8, 26712−26721

Table 1. Summary of the Time-Dependent GIWAXS Data of a Drop-Cast Perovskite Film at Different Temperatures

			crystallite size (nm)				
			intermediate product				
temperature (°C)	reaction period (min)	reaction time[a] (min)	PbI_2–solvent complex	$CH_3NH_3PbCl_3$	$CH_3NH_3PbI_{3-x}C_x$	degradation product PbI_2	stage of formation
70	0–8	8	64.42	54.87			I
	8–12	12	64.38	53.32			II
	>12	40	61.78	51.92	49.67		III
100	0–2	2	50.09	49.27	68.48		I
	2–4	4	48.23	48.08	67.96		II
	>4	40	46.94	46.76	34.99		III
140	0–12	5			54.87		III
	5–12	12			45.09	38.18	
	>12			all phases transform to amorphous structure			
180	0–3	0.5			65.77		III
	0.5–3	3			58.22	55.39	
	>3			all phases transform to amorphous structure			

[a]The time when the crystallite size was estimated.

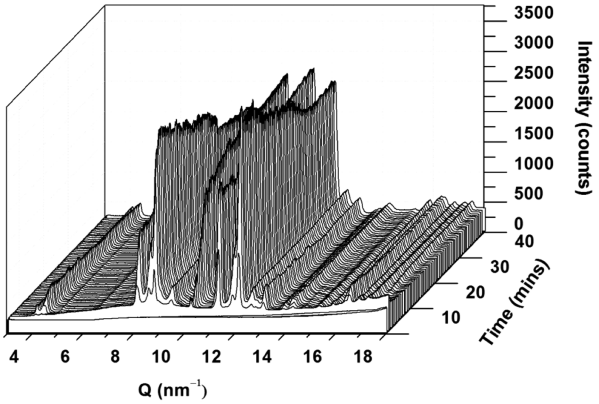

Figure 8. Time-dependent GIWAXS profiles of the perovskite film containing 1 wt % PEG drop-cast on the 100 °C substrate from solution to solid state (0–40 min).

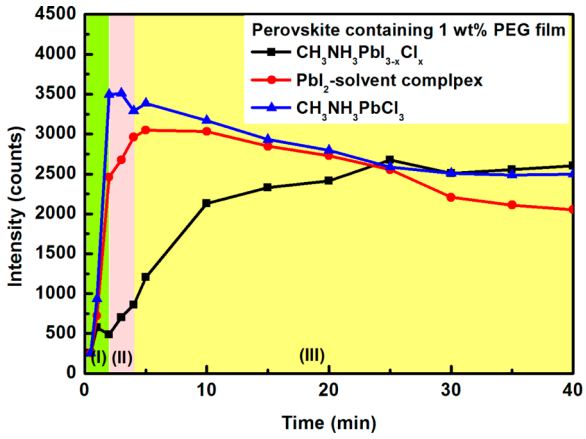

Figure 9. Variation of the peak intensities of the perovskite and intermediate phases corresponding to Figure 8 with time.

temperatures lower than 100 °C. Furthermore, high temperatures, >140 °C, promote faster, direct film formation, resulting in denser crystallites, larger grain size, and improved PCE.

This study also provides a fundamental understanding of solvent molecules that enhance the diffusion and reaction of precursors to assist the formation of intermediates and their transformation into a dry perovskite film in ambient conditions. Formation of the perovskite film from the precursor solution containing 1 wt % PEG also progresses through a three-stage formation mechanism at 100 °C. The presence of PEG can retard the growth of intermediates and stabilize the perovskite crystallites in the film. The planar perovskite solar cell based on the PEG-containing perovskite film therefore shows a better performance compared to the pristine perovskite film. A fundamental understanding of the crystallization behavior and phase transformation can provide a guideline to design an optimal one-step, drop-casting fabrication process for high-quality perovskite film in ambient conditions.

EXPERIMENTAL SECTION

Materials and Sample Preparation. The synthesis method of methylammonium iodide (CH_3NH_3I) was described elsewhere.[37] The 40 wt % pristine perovskite precursor solution was prepared by mixing CH_3NH_3I and lead chloride powder ($PbCl_2$; 99.999%, Aldrich) in a 3:1 molar ratio in an anhydrous *N*,*N*-dimethylformamide (DMF; 99.8%, Sigma-Aldrich) solvent. The perovskite precursor solution containing PEG additive is similar to the pristine one except by incorporation with 1 wt % PEG (Acros, MW = 6000). All of the precursor solutions were stirred at room temperature for at least 12 h before use.

Characterization. The in situ GIWAXS measurements were conducted on beamline 23A1 of the National Synchrotron Radiation Research Center, Taiwan.[32−36] The silicon substrate was placed on a temperature-controlled stage and then preheated to and maintained at 70, 100, 140, or 180 °C. All experiments were performed in air with a relative humidity of about 40%. The incident monochromated X-ray beam had a photon energy of 10 keV (a wavelength of 1.24 Å). After beamline alignment, the perovskite precursor solution was dropped onto the preheated silicon substrate and measurements were started immediately. The scattering signals were collected by a 2D X-ray detector with a sample-to-detector distance of 15.9 cm. The collection time for each measurement was 10 s. Each in situ measurement lasted 40 min. The one-dimensional (1D) GIWAXS profiles were reduced by the ring average from the 2D GIWAXS patterns. The fwhm values of the characteristic peaks were analyzed by the program *PeakFit v4.12*. Our previous study showed that the scattering intensity profile of the perovskite film on the silicon substrate was almost the same as that of perovskite on a TiO_2-coated silicon substrate, suggesting no substrate effect on the scattering profile.

DOI: 10.1021/acsami.6b07468
ACS Appl. Mater. Interfaces 2016, 8, 26712−26721

■ ASSOCIATED CONTENT

Supporting Information

The Supporting Information is available free of charge on the ACS Publications website at DOI: 10.1021/acsami.6b07468.

Time-dependent GIWAXS profiles of the pure iodide-based perovskite, selected 1D GIWAXS profiles, and peak assignments at different temperatures (PDF)

■ AUTHOR INFORMATION

Corresponding Authors

*E-mail: cstsao@iner.gov.tw (C.-S.T.).
*E-mail: suwf@ntu.edu.tw (W.-F.S.).

Notes

The authors declare no competing financial interest.

■ ACKNOWLEDGMENTS

The authors express their appreciation to the Ministry of Science and Technology of Taiwan (Grants MOST 104-3113-E-002-010 and 105-3113-E-002-010) for financial support and to Dr. Margaret M. S. Wu, Emeritus Senior Scientific Advisor of ExxonMobil Research and Engineering Co., for editing this manuscript.

■ REFERENCES

(1) Stranks, S. D.; Eperon, G. E.; Grancini, G.; Menelaou, C.; Alcocer, M. J. P.; Leijtens, T.; Herz, L. M.; Petrozza, A.; Snaith, H. J. Electron-Hole Diffusion Lengths Exceeding 1 Micrometer in an Organometal Trihalide Perovskite Absorber. *Science* **2013**, *342*, 341−344.

(2) Lee, M. M.; Teuscher, J.; Miyasaka, T.; Murakami, T. N.; Snaith, H. J. Efficient Hybrid Solar Cells Based on Meso-Superstructured Organometal Halide Perovskites. *Science* **2012**, *338*, 643−647.

(3) Noh, J. H.; Im, S. H.; Heo, J. H.; Mandal, T. N.; Seok, S. I. Chemical Management for Colorful, Efficient, and Stable Inorganic-Organic Hybrid Nanostructured Solar Cells. *Nano Lett.* **2013**, *13*, 1764−1769.

(4) Kim, H. S.; Lee, C. R.; Im, J. H.; Lee, K. B.; Moehl, T.; Marchioro, A.; Moon, S. J.; Humphry-Baker, R.; Yum, J. H.; Moser, J. E.; Grätzel, M.; Park, N. G. Lead Iodide Perovskite Sensitized All-Solid-State Submicron Thin Film Mesoscopic Solar Cell with Efficiency Exceeding 9%. *Sci. Rep.* **2012**, *2*, 591−597.

(5) NREL, http://www.nrel.gov/ncpv/, updated 8/12/2016.

(6) Heo, J. H.; Im, S. H.; Noh, J. H.; Mandal, T. N.; Lim, C.-S.; Chang, J. A.; Lee, Y. H.; Kim, H.-j.; Sarkar, A.; Nazeeruddin, M. K.; Grätzel, M.; Seok, S. I. Efficient Inorganic−Organic Hybrid Heterojunction Solar Cells Containing Perovskite Compound and Polymeric Hole Conductors. *Nat. Photonics* **2013**, *7*, 486−491.

(7) Wojciechowski, K.; Saliba, M.; Leijtens, T.; Abate, A.; Snaith, H. J. Sub-150 °C Processed Meso-Superstructured Perovskite Solar Cells with Enhanced Efficiency. *Energy Environ. Sci.* **2014**, *7*, 1142−1147.

(8) Docampo, P.; Ball, J. M.; Darwich, M.; Eperon, G. E.; Snaith, H. J. Efficient Organometal Trihalide Perovskite Planar-Heterojunction Solar Cells on Flexible Polymer Substrates. *Nat. Commun.* **2013**, *4*, 2761−2766.

(9) Kim, H. B.; Choi, H.; Jeong, J.; Kim, S.; Walker, B.; Song, S.; Kim, J. Y. Mixed Solvents for the Optimization of Morphology in Solution-Processed, Inverted-Type Perovskite/Fullerene Hybrid Solar Cells. *Nanoscale* **2014**, *6*, 6679−6683.

(10) Wang, K.; Liu, C.; Du, P.; Chen, L.; Zhu, J.; Karim, A.; Gong, X. Efficiencies of Perovskite Hybrid Solar Cells Influenced by Film Thickness and Morphology of $CH_3NH_3PbI_{3-x}Cl_x$ Layer. *Org. Electron.* **2015**, *21*, 19−26.

(11) Chiang, C. H.; Tseng, Z. L.; Wu, C. G. Planar Heterojunction Perovskite/$PC_{71}BM$ Solar Cells with Enhanced Open-Circuit Voltage Via a (2/1)-Step Spin-Coating Process. *J. Mater. Chem. A* **2014**, *2*, 15897−15903.

(12) Jiang, M.; Wu, J.; Lan, F.; Tao, Q.; Gao, D.; Li, G. Enhancing the Performance of Planar Organo-Lead Halide Perovskite Solar Cells by Using a Mixed Halide Source. *J. Mater. Chem. A* **2015**, *3*, 963−967.

(13) Ko, H. S.; Lee, J. W.; Park, N. G. 15.76% Efficiency Perovskite Solar Cells Prepared under High Relative Humidity: Importance of PbI_2 Morphology in Two-Step Deposition of $CH_3NH_3PbI_3$. *J. Mater. Chem. A* **2015**, *3*, 8808−8815.

(14) Im, J. H.; Jang, I. H.; Pellet, N.; Grätzel, M.; Park, N. G. Growth of $CH_3NH_3PbI_3$ Cuboids with Controlled Size for High-Efficiency Perovskite Solar Cells. *Nat. Nanotechnol.* **2014**, *9*, 927−932.

(15) Burschka, J.; Pellet, N.; Moon, S. J.; Humphry-Baker, R.; Gao, P.; Nazeeruddin, M. K.; Grätzel, M. Sequential Deposition as a Route to High-Performance Perovskite-Sensitized Solar Cells. *Nature* **2013**, *499*, 316−319.

(16) Bhachu, D. S.; Scanlon, D. O.; Saban, E. J.; Bronstein, H.; Parkin, I. P.; Carmalt, C. J.; Palgrave, R. G. Scalable Route to $CH_3NH_3PbI_3$ Perovskite Thin Films by Aerosol Assisted Chemical Vapour Deposition. *J. Mater. Chem. A* **2015**, *3*, 9071−9073.

(17) Luo, P.; Liu, Z.; Xia, W.; Yuan, C.; Cheng, J.; Lu, Y. Uniform, Stable, and Efficient Planar-Heterojunction Perovskite Solar Cells by Facile Low-Pressure Chemical Vapor Deposition under Fully Open-Air Conditions. *ACS Appl. Mater. Interfaces* **2015**, *7*, 2708−2714.

(18) Leyden, M. R.; Ono, L. K.; Raga, S. R.; Kato, Y.; Wang, S.; Qi, Y. High Performance Perovskite Solar Cells by Hybrid Chemical Vapor Deposition. *J. Mater. Chem. A* **2014**, *2*, 18742−18745.

(19) Chen, Q.; Zhou, H.; Hong, Z.; Luo, S.; Duan, H. S.; Wang, H. H.; Liu, Y.; Li, G.; Yang, Y. Planar Heterojunction Perovskite Solar Cells Via Vapor-Assisted Solution Process. *J. Am. Chem. Soc.* **2014**, *136*, 622−625.

(20) Li, Y.; Cooper, J. K.; Buonsanti, R.; Giannini, C.; Liu, Y.; Toma, F. M.; Sharp, I. D. Fabrication of Planar Heterojunction Perovskite Solar Cells by Controlled Low-Pressure Vapor Annealing. *J. Phys. Chem. Lett.* **2015**, *6*, 493−499.

(21) Ng, A.; Ren, Z.; Shen, Q.; Cheung, S. H.; Gokkaya, H. C.; Bai, G.; Wang, J.; Yang, L.; So, S. K.; Djurišić, A. B.; Leung, W. W.-f.; Hao, J.; Chan, W. K.; Surya, C. Efficiency Enhancement by Defect Engineering in Perovskite Photovoltaic Cells Prepared Using Evaporated PbI_2/CH_3NH_3I Multilayers. *J. Mater. Chem. A* **2015**, *3*, 9223−9231.

(22) Liu, M.; Johnston, M. B.; Snaith, H. J. Efficient Planar Heterojunction Perovskite Solar Cells by Vapour Deposition. *Nature* **2013**, *501*, 395−398.

(23) Zhou, H.; Chen, Q.; Li, G.; Luo, S.; Song, T. B.; Duan, H. S.; Hong, Z.; You, J.; Liu, Y.; Yang, Y. Photovoltaics. Interface Engineering of Highly Efficient Perovskite Solar Cells. *Science* **2014**, *345*, 542−546.

(24) Yang, W. S.; Noh, J. H.; Jeon, N. J.; Kim, Y. C.; Ryu, S.; Seo, J.; Seok, S. I. High-Performance Photovoltaic Perovskite Layers Fabricated through Intramolecular Exchange. *Science* **2015**, *348*, 1234−1237.

(25) Yu, H.; Wang, F.; Xie, F.; Li, W.; Chen, J.; Zhao, N. The Role of Chlorine in the Formation Process of"$CH_3NH_3PbI_{3-x}Cl_x$" Perovskite. *Adv. Funct. Mater.* **2014**, *24*, 7102−7108.

(26) Moore, D. T.; Sai, H.; Tan, K. W.; Smilgies, D.-M.; Zhang, W.; Snaith, H. J.; Wiesner, U.; Estroff, L. A. Crystallization Kinetics of Organic−Inorganic Trihalide Perovskites and the Role of the Lead Anion in Crystal Growth. *J. Am. Chem. Soc.* **2015**, *137*, 2350−2358.

(27) Nie, W.; Tsai, H.; Asadpour, R.; Blancon, J.-C.; Neukirch, A. J.; Gupta, G.; Crochet, J. J.; Chhowalla, M.; Tretiak, S.; Alam, M. A.; Wang, H.-L.; Mohite, A. D. High-Efficiency Solution-Processed Perovskite Solar Cells with Millimeter-Scale Grains. *Science* **2015**, *347*, 522−525.

(28) Tidhar, Y.; Edri, E.; Weissman, H.; Zohar, D.; Hodes, G.; Cahen, D.; Rybtchinski, B.; Kirmayer, S. Crystallization of Methyl Ammonium Lead Halide Perovskites: Implications for Photovoltaic Applications. *J. Am. Chem. Soc.* **2014**, *136*, 13249−13256.

DOI: 10.1021/acsami.6b07468
ACS Appl. Mater. Interfaces 2016, 8, 26712−26721

(29) Tan, K. W.; Moore, D. T.; Saliba, M.; Sai, H.; Estroff, L. A.; Hanrath, T.; Snaith, H. J.; Wiesner, U. Thermally Induced Structural Evolution and Performance of Mesoporous Block Copolymer-Directed Alumina Perovskite Solar Cells. *ACS Nano* **2014**, *8*, 4730−4739.
(30) Williams, S. T.; Chueh, C.-C.; Jen, A. K.-Y. Navigating Organo-Lead Halide Perovskite Phase Space via Nucleation Kinetics toward a Deeper Understanding of Perovskite Phase Transformations and Structure−Property Relationships. *Small* **2015**, *11*, 3088−3096.
(31) Dualeh, A.; Tetreault, N.; Moehl, T.; Gao, P.; Nazeeruddin, M. K.; Grätzel, M. Effect of Annealing Temperature on Film Morphology of Organic−Inorganic Hybrid Pervoskite Solid-State Solar Cells. *Adv. Funct. Mater.* **2014**, *24*, 3250−3258.
(32) Liao, H. C.; Tsao, C. S.; Lin, T. H.; Chuang, C. M.; Chen, C. Y.; Jeng, U. S.; Su, C. H.; Chen, Y. F.; Su, W. F. Quantitative Nanoorganized Structural Evolution for a High Efficiency Bulk Heterojunction Polymer Solar Cell. *J. Am. Chem. Soc.* **2011**, *133*, 13064−13073.
(33) Huang, Y. C.; Tsao, C. S.; Chuang, C. M.; Lee, C. H.; Hsu, F. H.; Cha, H. C.; Chen, C. Y.; Lin, T. H.; Su, C. J.; Jeng, U. S.; Su, W. F. Small- and Wide-Angle X-Ray Scattering Characterization of Bulk Heterojunction Polymer Solar Cells with Different Fullerene Derivatives. *J. Phys. Chem. C* **2012**, *116*, 10238−10244.
(34) Chen, C. Y.; Tsao, C. S.; Huang, Y. C.; Liu, H. W.; Chiu, W. Y.; Chuang, C. M.; Jeng, U. S.; Su, C. J.; Wu, W. R.; Su, W. F.; Wang, L. Mechanism and Control of the Structural Evolution of a Polymer Solar Cell from a Bulk Heterojunction to a Thermally Unstable Hierarchical Structure. *Nanoscale* **2013**, *5*, 7629−7638.
(35) Liao, H. C.; Tsao, C. S.; Lin, T. H.; Jao, M. H.; Chuang, C. M.; Chang, S. Y.; Huang, Y. C.; Shao, Y. T.; Chen, C. Y.; Su, C. J.; Jeng, U. S.; Chen, Y. F.; Su, W. F. Nanoparticle-Tuned Self-Organization of a Bulk Heterojunction Hybrid Solar Cell with Enhanced Performance. *ACS Nano* **2012**, *6*, 1657−1666.
(36) Liao, H. C.; Tsao, C. S.; Shao, Y. T.; Chang, S. Y.; Huang, Y. C.; Chuang, C. M.; Lin, T. H.; Chen, C. Y.; Su, C. J.; Jeng, U. S.; Chen, Y. F.; Su, W. F. Bi-Hierarchical Nanostructures of Donor−Acceptor Copolymer and Fullerene for High Efficient Bulk Heterojunction Solar Cells. *Energy Environ. Sci.* **2013**, *6*, 1938−1948.
(37) Chang, C. Y.; Chu, C. Y.; Huang, Y. C.; Huang, C. W.; Chang, S. Y.; Chen, C. A.; Chao, C. Y.; Su, W. F. Tuning Perovskite Morphology by Polymer Additive for High Efficiency Solar Cell. *ACS Appl. Mater. Interfaces* **2015**, *7*, 4955−4961.

DOI: 10.1021/acsami.6b07468
ACS Appl. Mater. Interfaces 2016, 8, 26712−26721